Challenging Glass Conference Proceedings – Volume 9 – June 2024 – Louter, Bos & Belis (Eds.)
International Conference on the Architectural and Structural Application of Glass
Challenging Glass Conference 9 – 19 & 20 June 2024 – TU Delft – The Netherlands

Adhesion of Laminated Glass Interlayers in a Double Cantilever Beam Test

Paul Elzière [a], Yael Bronstein [a], Fabien Levasseur [a], Francis Serruys [b]

a Saint-Gobain Glass France
b Saint-Gobain Innovative Materials Belgium

Abstract

Laminated glass is a key safety element in modern building with glass façades. Tuning the adhesion between the interlayer and the glass as well as the mechanical properties of the interlayer are essentials to both the quality of the laminated glass manufacturing and to the final performance, especially regarding their wind-load and impact resistance. Adhesion tests conducted on laminated glass include pure shear and tensile loading tests. However, certain assembly geometry and framing systems lead to more complex loadings being applied on the laminated glass. We focus in this study on the Double Cantilever Beam (DCB) test that models one of these configurations. We compared three different types of typical interlayers used in the building industry, a standard Poly Vinyl Butyral (PVB), a structural PVB and an ionomer interlayer. We conducted tests at different temperatures and loading speeds to screen a broad range of conditions seen by the interlayer in the field. We found that the nature of the interlayer has a dramatic impact on the measured adhesion to glass which is directly linked to its mechanical properties and to the experimental conditions. In the specific loading conditions of the DCB test, we have identified for each interlayer, a regime of low adhesion levels combined to a rapid propagation of the delamination front under certain temperatures and loading speeds.

Keywords

Glass, Laminated, Interlayer, Adhesion, DCB

Article Information

- Digital Object Identifier (DOI): 10.47982/cgc.9.543
- Published by Challenging Glass, on behalf of the author(s), at Stichting OpenAccess.
- Published as part of the peer-reviewed Challenging Glass Conference Proceedings, Volume 9, June 2024, 10.47982/cgc.9
- Editors: Christian Louter, Freek Bos & Jan Belis

1. Introduction

The interlayer adhesion to glass and its mechanical behavior are directly linked to the performance of the laminated glass with respect to impact, wind loads or static loads. To study the glass adhesion of different interlayers, several tests can be used. In the industry, some commonly found tests include the pummel test described in ASTM C1908-21 or in the literature (Schuster, et al., 2020), the shear torsion adhesion test as mentioned in (Decourcelle, 2011), or the pull test (Chung & Chaudury, 2005; Santarsiero, et al., 2017). Standard adhesion tests such as 90° peel test (Huntsberger, 1981; Pelfrene, et al., 2015) have also been used to characterize the adhesion of the glass and the interlayer. Shear geometries such as compressive shear test (Rahul-Kumar, et al., 2000; Jagota, et al., 2000) or double lap shear test (Centelles, et al., 2020; Biolzi, et al., 2014) have also been used. Through Crack Tensile (TCT) Test has been extensively used to mimic broken glass bridged by the interlayer after impact (Sha, et al., 1997; Seshadri, et al., 2002; Delince, et al., 2008; Ferretti, et al., 2012; Butchart & Overend, 2012; Samieian, et al., 2019). Indeed, the TCT Test proved useful to understand dissipation mechanisms during an impact (Elziere, et al., 2017; Fourton, et al., 2020).

However, in certain applications, the edges of the laminated glass panels can be submitted to cleavage opening. The interlayer is submitted in this configuration in a load that cannot be reproduced by shear tests or TCT tests and that cannot be captured properly by simple pull tests or peel tests. The Double Cantilever Beam (DCB) test is used most of the time to test the adhesion of structural adhesives ASTM D3433-99 (Blackman & Kinloch, 2001; Blackman, et al., 2000). We found that this testing method is the closest to this type of cleavage load scenarios. (Poblete, et al., 2022) recently presented some DCB test results on laminated glass. However, because these cleavage loading scenarios are rather rare, there is less literature regarding the use of the DCB test to characterize adhesion of interlayers in laminated glass.

We used the DCB test to quantify the adhesion between three interlayers: a standard Poly Vinyl Butyral (PVB), a structural PVB and an ionomer interlayer, at different temperatures and speeds relevant for building façade applications. We also tried to explain the difference in delamination mechanisms and adhesion energy using rheological data available in the literature.

2. Experiments

2.1. Materials

In this study we compared 3 different interlayers commonly used in the building glass industry:

- A standard PVB interlayer commonly used in building applications.
- A structural PVB also called stiff PVB interlayer in the literature.
- An ionomer interlayer.

To be representative of normal production practices the PVB interlayers are assembled in a configuration where one side faces the atmospheric side of the glass and the other faces the tin side of the glass. The ionomer interlayer is assembled in a configuration where both tin faces of the glass are in contact with the interlayer as recommended by the manufacturer. No primers were used in this assembly.

The glass used in these experiments is a clear glass without coating. The glass is cut, and the edges are finished before tempering. Tempered glass is used to improve the flexion resistance of the beams in the DCB test.

2.2. DCB samples geometry and testing equipment

Figure 1 gives a side schematic view of the samples as well as pictures of the test setup. The samples are based on beams of tempered clear glass with no coating. The beams are L=300mm long, w=50mm wide and h=8mm thick.

The interlayers standard PVB, structural PVB and ionomer all have a thickness of h_i=0.76mm.

An initial gap of 100mm length is left without interlayer between the two glass beams at one end of the sample. The displacement is applied at 25mm of the edge of the beam above that gap. We thus consider in the calculations an initial crack length a_0 = 75mm. We apply the displacement at controlled speed v.

The displacement is applied through a metal puck that is glued to the glass surface using a metacrylate structural glue. The bottom metal clam is fixed while the displacement is applied on the upper metal clamp.

During the loading we record the force using a 5kN cell on an Instron 2525 machine.

Loading conditions temperatures and loading speeds are defined in Section 2.4.

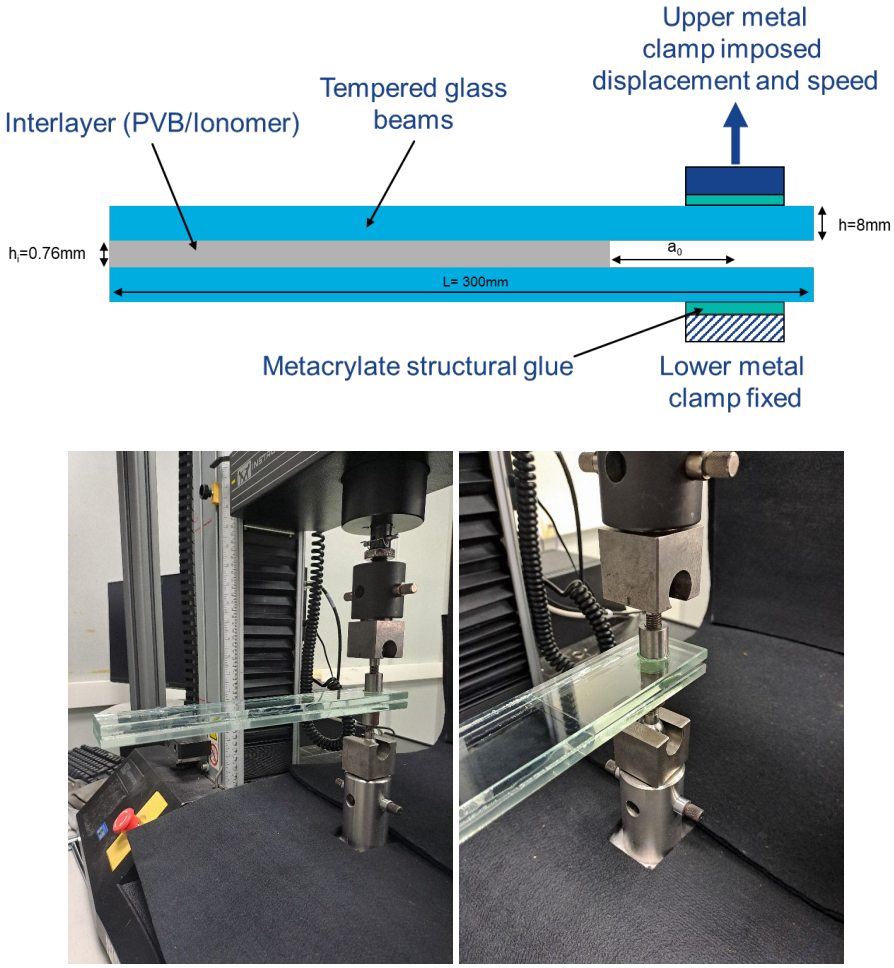

Fig. 1: Geometry of the Double Cantilever Beam samples (top).
Pictures of the samples and fixture on the tensile testing machine (bottom).

2.3. Assembly and autoclave cycles

Interlayers are stored for several weeks at controlled temperature and humidity before assembly 20°C/20%HR. Assembly is performed in a clean room environment at controlled temperature and humidity (16°C/30%RH).

A small PTFE plate is inserted inside the empty space at the front of the sample to avoid overflow of the interlayer during lamination. This is especially critical for the ionomer interlayer that tends to flow outside of the sample edges during lamination. To limit even more the overflowing of the ionomer interlayer, silicon bands are also taped all around the edges of the sample. During the autoclave cycle, the glass/interlayer assembly is maintained in position using temperature resistant tape.

Samples are first put in a sealed vacuum bag at room temperature. The assembly is then finalized in an autoclave with temperature and pressure cycles specific to the interlayers.

For the standard and structural PVB, the samples are submitted to a standard industrial PVB lamination cycle which is given in Figure 2.

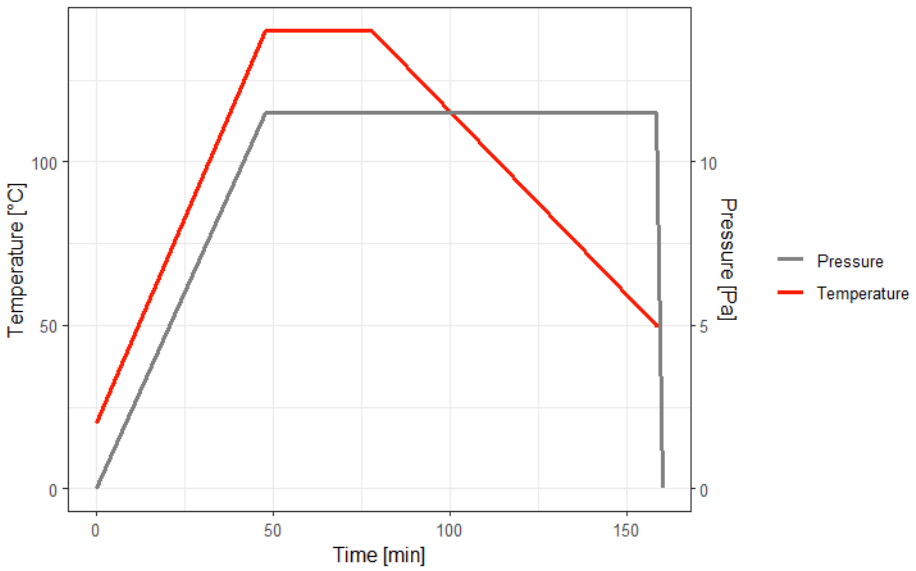

Fig. 2: Autoclave cycle for assembly of standard and structural PVB interlayers.

For the ionomer the samples are autoclaved with the cycle in Figure 3 recommended by the manufacturer.

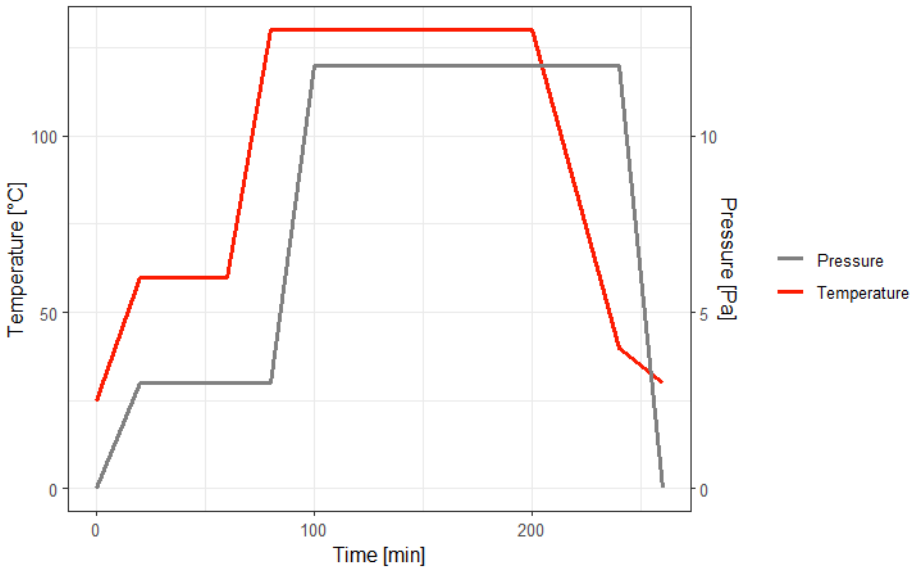

Fig. 3: Autoclave cycle used for assembly of the ionomer interlayer.

2.4. Conditions of testing

Samples are tested in a range of displacement speeds between 0.1mm/min and 60mm/min.

Samples are conditioned at a set temperature before the test. The test only last for a few minutes but the temperature of the samples tends to equilibrate slowly with the room temperature. We thus measured an approximate value of the sample temperature using an infrared thermometer. We use this temperature as a label for the different conditions. The laboratory temperature is controlled at 20°C.

The test temperatures are labeled as follows:

- Labeled -10°C samples are stored in a freezer at -18°C overnight before the test.
  The temperature of the samples during the test is in between -10°C and -5°C.
- Labeled 10°C samples are stored in a fridge at 0°C overnight before the test.
  The temperature of the samples during the test is in between 5-10°C.
- Labeled 20°C samples are simply stored at room temperature.
- Labeled 40°C samples are heated at 50°C for a few hours and then tested.
  The temperature of the samples during the test is about 35-40°C.
- Labeled 50°C samples are heated for a few hours at 55°C and tested immediately.
  Measured temperature was between 45 and 50°C.
- Labeled 80°C samples are heated at for a few hours and tested immediately.
  The measured temperature is close to 75°C.

The table below summarizes the testing conditions and the number of samples tested per condition.

Table 1: Testing conditions and number of samples tested per condition.

Temperature Label °C	Speed mm/min	Interlayer	Number of samples
-10	1	Structural PVB	5
-10	1	Standard PVB	5
-10	1	Ionomer	5
-10	60	Structural PVB	5
-10	60	Standard PVB	5
10	1	Standard PVB	4
10	1	Ionomer	5
10	6	Structural PVB	10
10	6	Standard PVB	13
10	60	Standard PVB	3
20	0.1	Standard PVB	9
20	1	Structural PVB	5
20	1	Standard PVB	7
20	1	Ionomer	4
20	6	Structural PVB	4
20	60	Structural PVB	5
20	60	Standard PVB	5
20	60	Ionomer	4
40	1	Structural PVB	6
40	1	Standard PVB	5
40	1	Ionomer	5
40	60	Standard PVB	6
50	1	Ionomer	5
80	1	Ionomer	4
80	60	Ionomer	5

3. Results

3.1. 2 delamination regimes

Our first observation at room temperature and at a speed of 1mm/min already shows different delamination mechanisms between the different interlayers.

The ionomer and the structural interlayer delaminate abruptly with little deformation of the interlayer (Figure 4). The crack propagates at a critical load over several centimeters. In the rest of the paper, we will call this regime, the abrupt delamination regime.

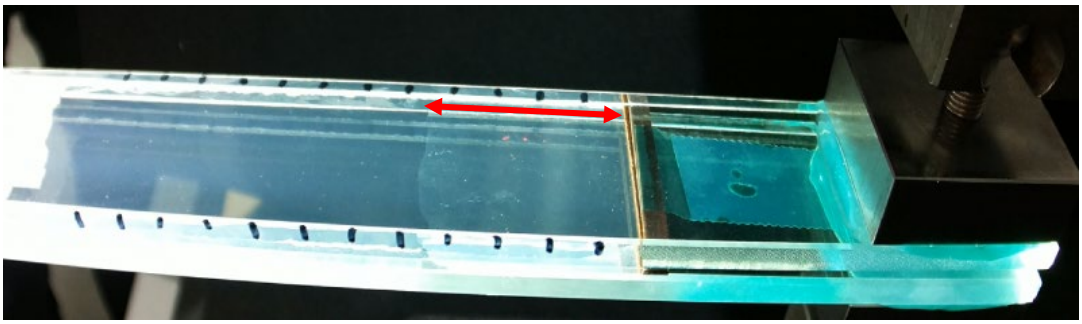

Fig. 4: For the structural interlayer and the ionomer, at room temperature and at a speed of 1mm/min, the delamination front propagates abruptly over several centimeters. On the picture we can see the delamination front that has propagated between its initial position and the position visible here (red arrow ~4cm) within a fraction of seconds.

The forces measured in that regime are typically below 600N. Figure 5 shows the load vs cross head displacement curve for the ionomer at room temperature and 1mm/min, these curves are typical of the abrupt delamination regime.

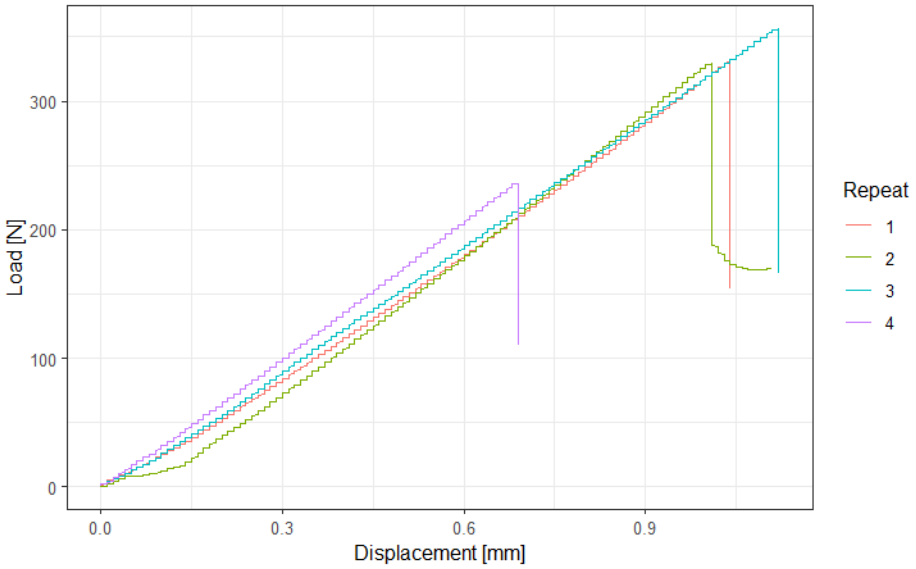

Fig. 5: Load vs. Displacement curves for the ionomer. Typical curves observed in the abrupt delamination regime.

In contrast, samples with standard PVB, exhibit a delamination front that propagates at a constant speed, when tested at room temperature and 1mm/min. The interlayer is stretched at least to 100% strain, cavitation bubbles can be observed ahead of the delamination front over a distance of a few centimeters (Figure 6). It is unclear if these are nucleated inside the bulk material or at the interface

with the glass. The cavitation zone travels at the same speed ahead of the delamination front. In the rest of the paper, we will call this regime, the large deformation delamination regime.

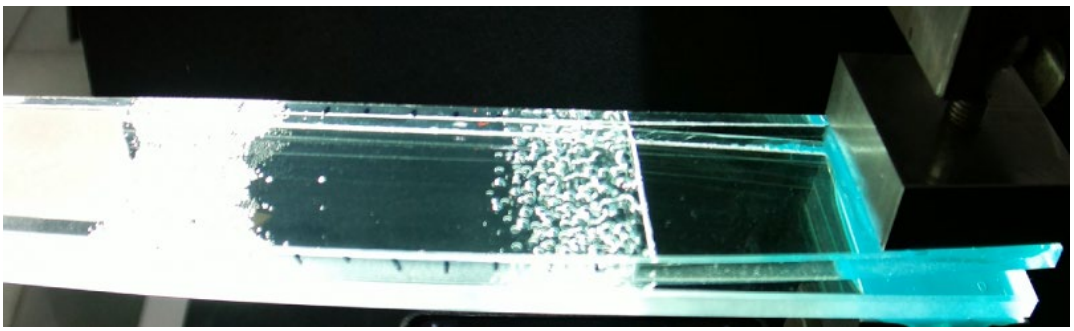

Fig. 6: At room temperature and at a speed of 1m/min, the standard PVB interlayer delaminates in relatively slow propagation of the delamination front. A steady state regime in which the delamination is occurring with a large deformation of the interlayer and cavitation ahead of the delamination front.

The forces in that regime are typically above 500-600N. Figure 7 shows the load vs crosshead displacement curve for the standard PVB at room temperature and 1mm/min. These curves are representative of the large deformation delamination regime. The crosshead displacement results in a stretching of the interlayer. One can see that one of the curves end abruptly with the load decreasing rapidly before a steady state can be completely observed. This is due to the breakage of the tempered glass beam due to the high deflection required to propagate the delamination front.

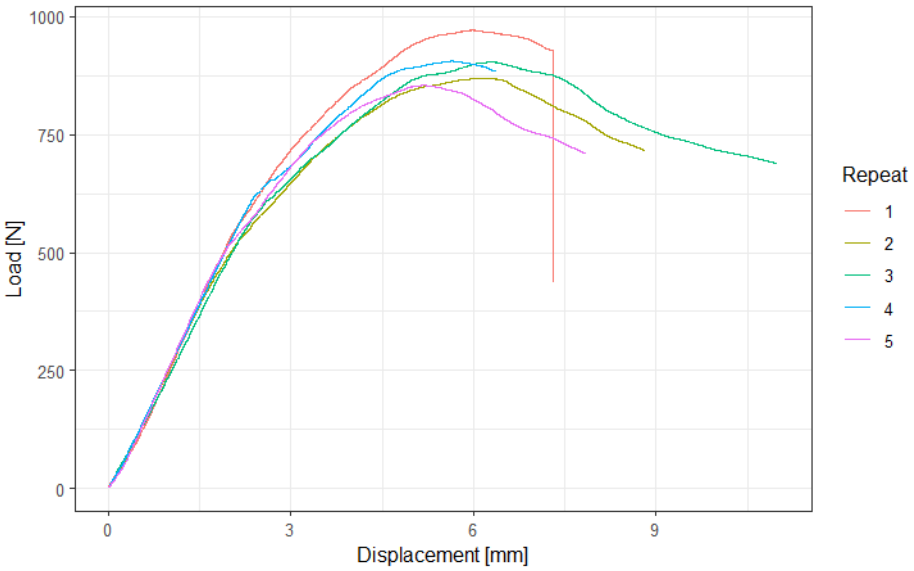

Fig. 7: Load vs. Displacement curves for the standard PVB.
Typical curves observed in the large deformation delamination regime.

These 2 regimes of delamination can be observed at different temperatures and loading speeds for all 3 interlayers as we will discuss in 3.4.

In Figure 8, we show the load displacement curves at 20°C and 60mm/min where the standard PVB is in the large deformation delamination regime while both the structural PVB and the ionomer interlayer are in the abrupt delamination regime.

The large delamination force seen with the standard PVB is due to the large deformation of the interlayer over a relatively large zone of cavitation ahead of the delamination front. The delamination

front only starts to propagate after the maximum load is reached. The steady state delamination leads to a small decrease in the measured load. The test was stopped after some time to avoid breaking the glass beams. This can occur when the deflection of the beam is too important. We can see an occurrence of such breakage in one of the samples of standard PVB where the load decreases abruptly when the glass beam broke.

The smaller delamination force observed for the structural PVB and ionomer are due to the smaller stretching of the interlayer. We can also observe evidence of the abrupt propagation of the delamination front when the load abruptly decreases after reaching a critical value.

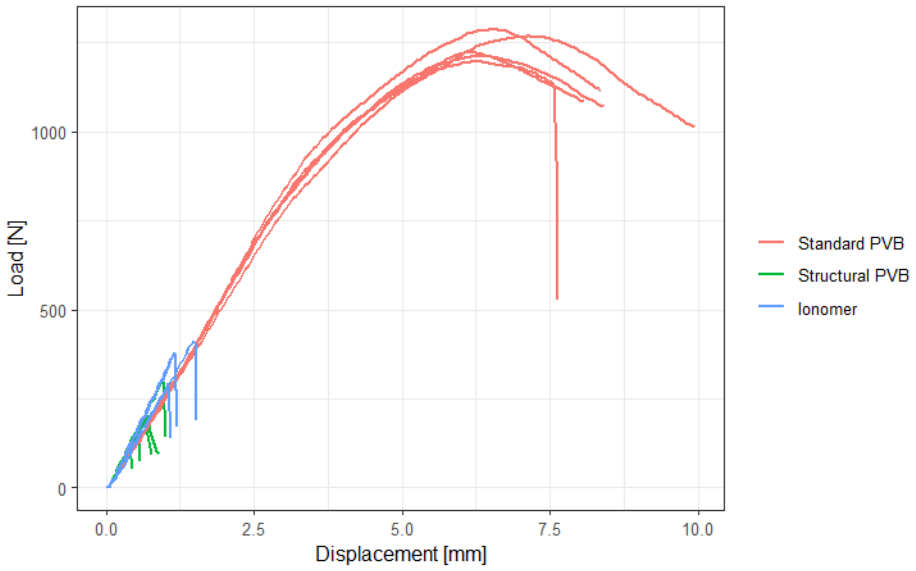

Fig. 8: At 20°C and 60mm/min both the structural PVB and Ionomer are in the abrupt delamination regime while the standard PVB is in the large deformation delamination regime.

3.2. Force measurement

The maximum load, which corresponds to the peak of the curve, is recorded for every experiment (Figure 9). We present here the results as a box plot. In these plots, the middle line of the box is the median value of the experiment, the bottom and top hinges represent respectively the first and the third quartiles of the distribution and the whiskers are extending from the hinge limit to 1.5 times the IQR (inter quartile range). Data beyond the whiskers are outlying points which are displayed individually as black points.

We were not able to consistently record the onset of delamination force in the large deformation delamination regime as the adhesion was high enough to lead to the glass beam breakage. This also means the highest values of the load that we recorded (typically above 1000N) are limited by the strength of the tempered glass beam and are not a true measurement of the adhesion between the interlayer and the glass. This happened for the following conditions:

- Standard PVB at 20°C 1mm/min and 60mm/min
- Structural PVB at 40°C and 1mm/min
- Ionomer at 50°C 1mm/min and 80°C 1 and 60mm/min

In Figure 9, it is difficult to interpret the variations of the measured load with the temperature and the speed. We need to convert the load into an adhesion energy and the speed into a characteristic time (Section 3.3) so that we can link the behavior observed in the DCB experiment with the rheology of the interlayers (Section 3.4).

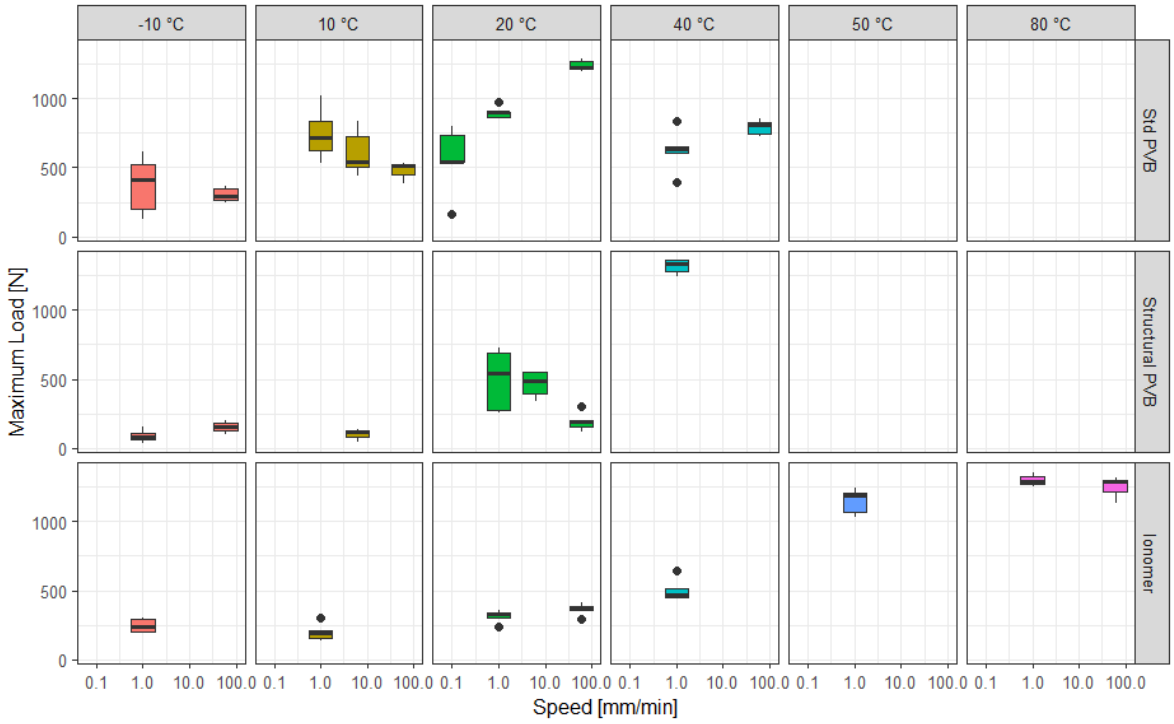

Fig. 9: Maximum load recorded at different loading speeds and temperature. In these plots, the middle line of the box is the median value of the experiment, the bottom and top hinges represent respectively the first and the third quartiles of the distribution and the whiskers are extending from the hinge limit to 1.5 times the IQR (inter quartile range). Data beyond the whiskers are outlying points which are displayed individually as black points. The highest loads above 1000N observed for the highest adhesion are typically limited by the strength of the tempered glass beam. Note that we did not performed any tests for the standard and structural PVB at 50°C and 80°C.

3.3. DCB Adhesion Energy dependence on the temperature and loading speed.

Based on the maximum load measurements, we can estimate the energy release rate or adhesion energy G_c using the following equation (Mostovoy, 1966; Blackman & Kinloch, 2001):

$$G_c = \frac{4P_{max}^2}{Ew^2}\left(\frac{3a_0^2}{h^3}+\frac{1}{h}\right)$$

Where P_{max} is the maximum load (the peak of the force vs. displacement curve), E=70GPa is the modulus of the glass, w=50mm is the width of the beam, h=8mm is the thickness of the glass beam and a_0=75mm is the initial crack length.

In Figure 10, we present the adhesion energy measured in the DCB test at different loading speeds and temperatures. The temperature labels in this figure are only indicative of the average temperature. We use in this figure a characteristic time of loading on the x-axis which is given by the ratio of the interlayer thickness h_i=0.76mm and the loading speed v. Note that the characteristic time of loading is in the same order of magnitude than the typical load durations used for wind loads calculations on façade applications as described in EN 16612:2019 (wind load gust 5s and cumulative wind storm load 10min).

(Poblete, et al., 2022) have also performed DCB experiments on standard PVB at room temperature and at different load speeds. They also noted an interfacial delamination. We can compare the results obtained by the authors at 0.3mm/min and 1.2mm/min with an interlayer of 0.3mm thickness. These two loading speeds correspond to characteristic times of 60s and 15s respectively. The maximum load obtained by Poblete et al. are about 3.2kN at 0.3mm/min – 60s and 4.5kN at 1.2mm/min -15s. Considering the difference of geometry and sample constructions we can estimate the adhesion energy to be 1.2kJ/m² for a characteristic time of 15s and 0.7kJ/m² for a characteristic time of 60s which aligns quite well with our own measurements at 20°C on standard PVB.

The adhesion energy in the DCB experiment, at low temperature relative to the glass transition and for the characteristic times tested here, falls below 0.2kJ/m² which is a typical value for the transition between the two delamination regimes described in Section 3.1. It is important to note that the ionomer presents an adhesion energy below 0.2kJ/m² over a broad range of typical application temperatures between -10 to 40°C. On the contrary, the standard PVB, has an adhesion energy above this value over a broader range of typical application temperatures between 10 and 40°C but also falls below this limit at -10°C. Finally, the structural PVB interlayer has an adhesion energy below the 0.2kJ/m² limit over a range of -10°C to ~20°C.

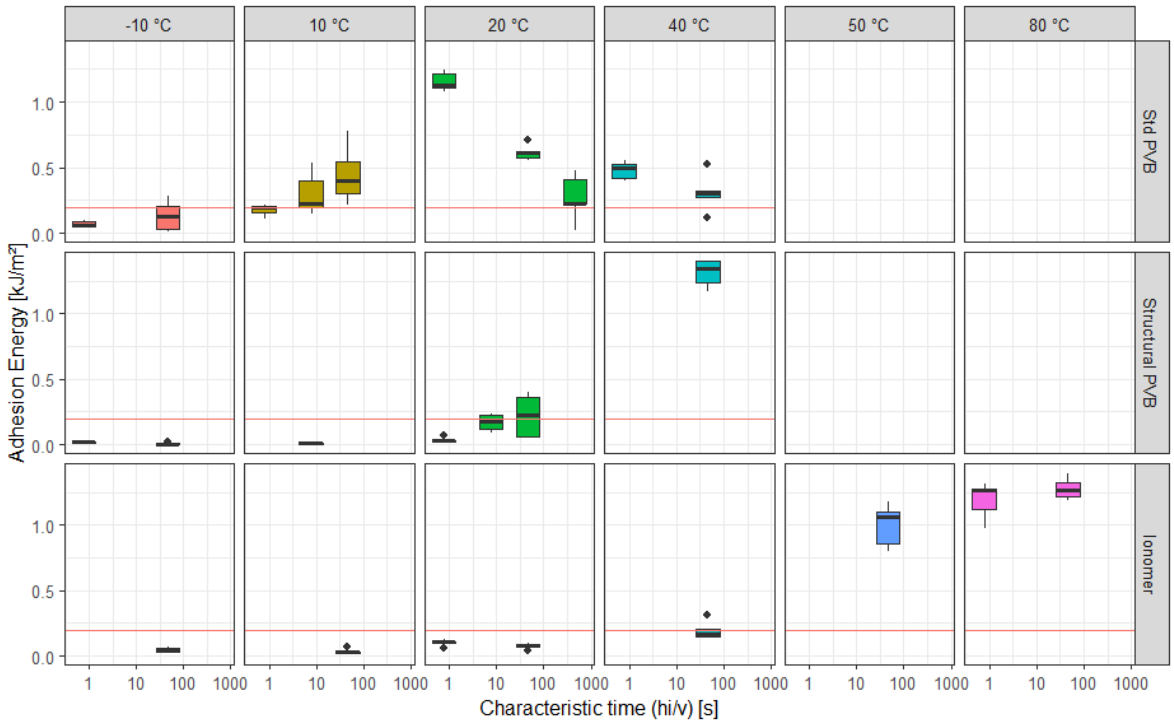

Fig: 10: temperature and loading speed dependence of the DCB adhesion energy. The x axis is a characteristic time which is given by the ratio of the interlayer thickness (0.76mm) and the loading speed. The interlayer adhesion energy increases by an order of magnitude as we get close to its glass transition temperature (see Section 3.4). We can see on the ionomer samples that the adhesion energy is kept at high value after the glass transition. For the standard interlayer on the contrary, the adhesion energy decreases after the glass transition.

3.4. Discussion - Link with the interlayer rheology

It is well known that laminated glass interlayers whether standard PVB, structural PVB or ionomer based have a mechanical behavior that depends on the temperature and speed as shown in many previous studies such as (Centelles, et al., 2021; Briccoli Bati, et al., 2009; Santarsiero, et al., 2016; Stevels, et al., 2016; Corroyer, et al., 2013; Hooper & Blackman, 2012; Juang, et al., 2001) and (Biolzi, et al., 2020; Moreno, et al., 2022; Yang, et al., 2023; Elziere, et al., 2019).

The glass transition occurs rather over a broad range of temperatures for the three different interlayers. In the literature the glass transition can be, among other methods, identified using DMA. We can find the following range of temperatures for the glass transitions of the different interlayers (temperature ramp experiments in the small deformation regime at 1Hz):

- Standard PVB 20-30°C (Stevels, et al., 2016; Moreno, et al., 2022)
- Structural PVB 30-50°C (Stevels, et al., 2016; Decourcelle, et al., 2009)
- Ionomer 35-55°C (Xie, et al., 2024)

We can see in Figure 10, that the time/temperature superposition usually found in the interlayer rheology studies, can also be applied here. Indeed, we obtain a curve like the time/temperature superposition master curves where shorter characteristic times are equivalent to colder temperatures.

As the interlayer gets close to its glass transition the delamination mechanism changes. We observe the transition from the abrupt delamination regime with very little deformation of the interlayer, to the large deformation delamination regime with large bulk deformation of the interlayer, cavitation, and relatively slow steady state delamination.

We can find in the literature different Maxwell models describing the different interlayers. In (Centelles, et al., 2021), relaxation experiments on standard PVB; structural PVB and ionomer are performed in a tensile DMTA apparatus, at different temperatures between -10°C and 50°C. (Stevels, et al., 2016) performed shear plane/plane frequency sweep on standard PVB and structural PVB with frequency ranging between 0.1 and 100rad/s and with temperatures in-between -30°C to 90°C. (Moreno, et al., 2022) conducted relaxation experiments on standard PVB between 60°C and 140°C but also frequency sweep experiments between 0.1 to 10rad/s and temperatures ranging between 20°C and 140°C. The authors used here a plane/plane shear rheometer geometry. In (Elziere, 2016), both tensile DMA and plane/plane rheology were combined to perform frequency sweeps on standard PVB between 0.1 and 10Hz with temperature ranging overall from -40°C to 160°C. (Xie, et al., 2024) used tensile DMA to perform frequency sweeps between 0.1 and 10 rad/s and temperature ranging between -50 to 55°C for standard PVB and -50°C to 120°C for Ionomer interlayer. In all these studies, the time/temperature superposition principle was used to obtain master curves of elastic modulus vs. time for the different interlayers.

A generalized Maxwell model (Wiechter., 1893) was used to fit these master curves and the WLF law coefficients (Williams, et al., 1955) C_1 and C_2 are given to shift the curves at different temperatures:

$$\log(a_T) = \frac{-C_1(T - T_{ref})}{C_2 + T - T_{ref}}$$

Note that the Maxwell model is describing the rheology of the interlayer in the linear viscoelastic range. Its use in this context, where the interlayer can stretch outside the linear viscoelastic range, is only qualitative.

Using the coefficient from the Prony series given in the previously cited papers we can calculate the modulus at a given characteristic time and a given temperature matching our DCB experiments:

$$E(t,T) = E_\infty + E_0 \sum E_i e^{-t/a_T \tau_i}$$

Where E_i and τ_i are the terms of the Prony series of the Maxwell model, E_∞ is the long-term modulus and E_0 is the instantaneous modulus. Note that we converted shear modulus to tensile modulus using the relationship:

$$E = 2\mu(1+\nu) \sim 3\mu$$

Where μ is the shear modulus and E the tensile modulus and $\nu \sim 0.5$ is an approximate of the Poisson coefficient of the interlayer considered constant over the temperature range of the rheology tests.

Figure 11 shows the calculated modulus for the different models, conditions, and interlayers. We added in red a first limit at 100MPa that seems to match the onset of larger deformation of the interlayer during the DCB test but with no visible cavitation. In blue, the second limit at 10MPa seems to correspond to the onset of cavitation, large deformation, and high level of adhesion (>0.5kJ/m²).

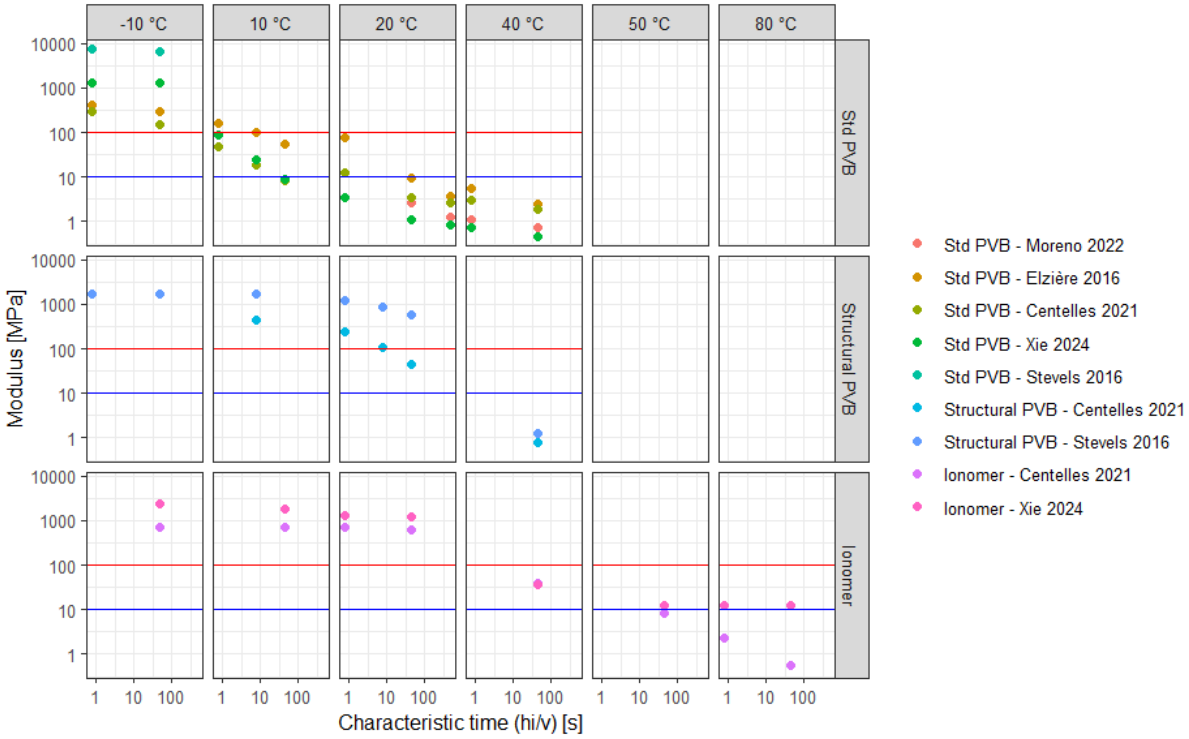

Fig. 11: Modulus calculated from Maxwell model data found in the literature (Moreno, et al., 2022) (Xie, et al., 2024) (Centelles, et al., 2021) (Elziere, 2016). The red line at 100MPa seems to match the transition between the abrupt delamination regime and the large deformation regime although no cavitation is yet visible. The blue line at 10MPa seems to match the onset of cavitation and the ramp up to high adhesion energies (>0.5kJ/m²).

The storage modulus E' and loss modulus E'' can be calculated at different frequencies and temperatures using the following relationships:

$$E'(\omega, T) = \sum E_i \frac{\omega^2 a_T \tau_i^2}{1 + \omega^2 a_T \tau_i^2}$$

$$E''(\omega, T) = \sum E_i \frac{\omega a_T t_i}{1 + \omega^2 a_T t_i^2}$$

With ω the frequency that we defined for each characteristic times h_i/v as $\omega = \pi v/h_i$. This is an approximation of the characteristic frequency corresponding to half an oscillation as we are only loading the material and not doing cyclic loading/unloading. The frequency is used to calculate both the storage and loss modulus at a given characteristic time and temperature of the DCB experiments. We use these values to calculate the loss factor $\tan(\delta) = E''/E'$ for each temperature and characteristic time. For clarity in Figure 12, we only represent data using the models from (Centelles, et al., 2021) which were available for all 3 types of interlayers. The peak of the loss factor can be indicative of the glass transition.

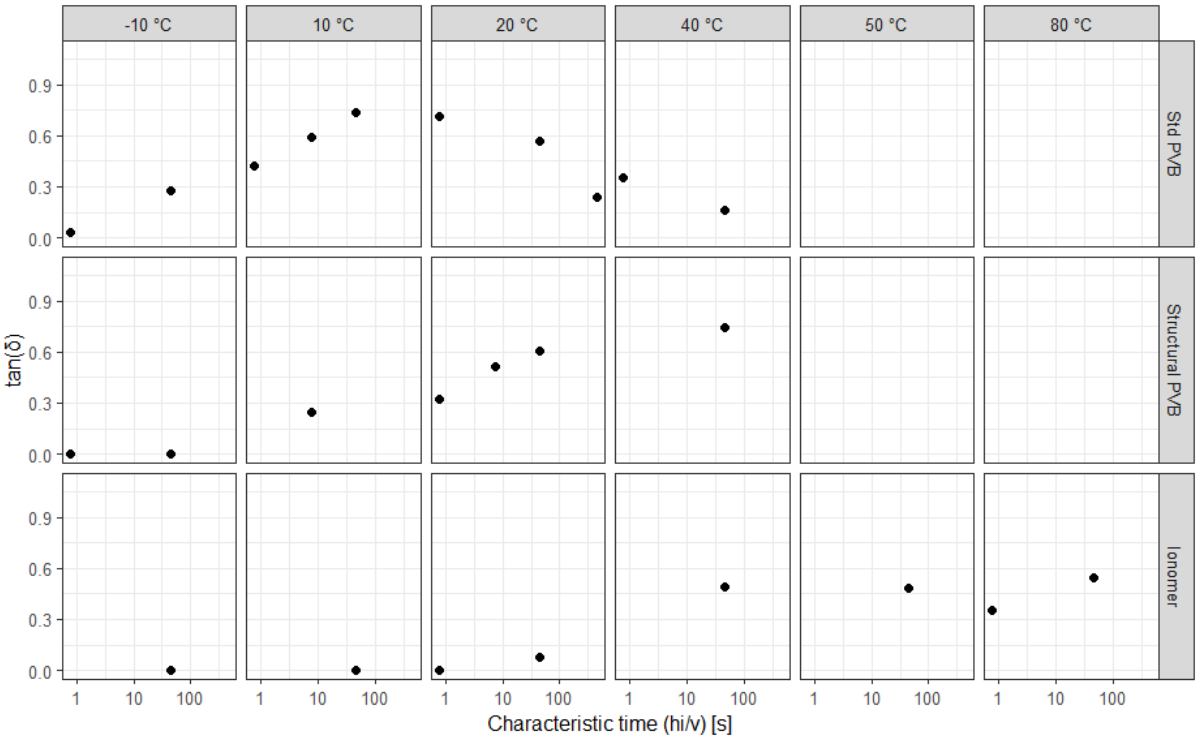

Fig. 12: Loss factor calculated from the data of (Centelles, et al., 2021) for each temperature and corresponding characteristic time to the DCB experiment.

Figure 13 shows the adhesion energy as a function of $\tan(\delta)$ for each interlayer. The color of the points is indicating the temperature of the test while the shape indicates the characteristic times. We can clearly identify a relationship between an increase in adhesion energy and the increase in loss factor:

- For the standard PVB we can see that at first, as the temperature increases and the characteristic time lengthens, the loss factor increases, the polymer enters the glass transition, and the adhesion energy also increases. Then, when the interlayer exits the glass transition for higher temperature or even longer characteristic times, the loss factor goes back down, and the adhesion energy decreases as well.
- For the structural PVB, our experiments stop at 40°C, we can only observe the first part of the curve where the interlayer enters the glass transition as the temperature increases and the characteristic time lengthens. The adhesion energy increases with the loss factor as observed with the standard PVB. We can anticipate that a similar behavior to the one observed with the standard PVB will be observed beyond the glass transition, the loss factor and the adhesion energy will decrease.
- For the ionomer, the behavior is slightly different. At 40°C and 0.76s, the loss factor already increased but the adhesion energy is still relatively low. Only after reaching 50°C, we see an increase in adhesion energy. Interestingly both the loss factor and the adhesion energy are staying relatively high even at 80°C. This could indicate a different dissipation mechanism in the ionomer interlayer which is known to have crystallites (Su, et al., 2022; Schuster, 2022) melting at this temperature of 80°C and additionally present a plastic dissipation mechanism at large strain (Santarsiero, et al., 2016).

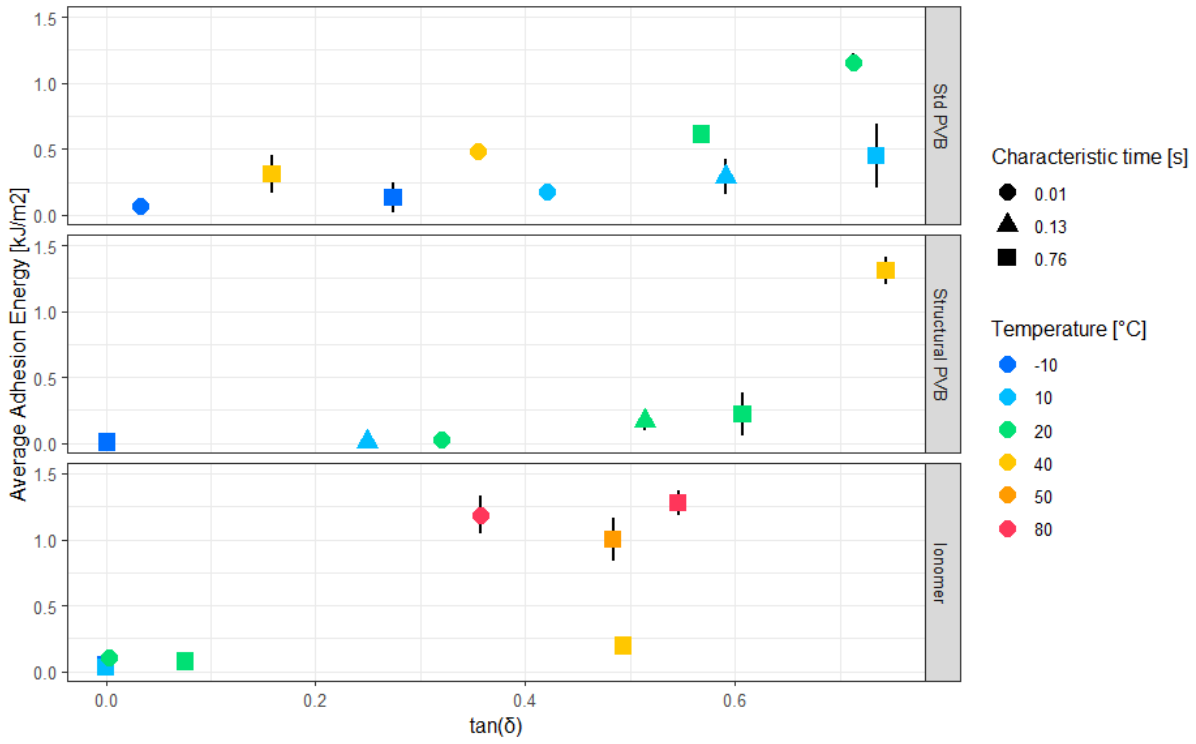

Fig. 13: Average adhesion energy estimated for each speed and temperature as a function of the loss factor of the interlayer for the corresponding characteristic time/frequency. For the PVB interlayers both standard and structural, there is a clear correlation with an increase in loss factor resulting in higher adhesion energy. For the ionomer, the adhesion energy increases initially with the loss factor when the temperature increases but then it plateaus at a high level after when the temperature is above the glass transition.

4. Conclusion

We used the DCB test to characterize the adhesion of 3 different interlayers. We first observed 2 delamination regimes:

- an abrupt delamination regime at high speed and low temperature relative to the glass transition.
- a high deformation delamination regime at lower speeds and higher temperatures when getting closer or above the glass transition. This regime is characterized by the large deformation of the interlayer and cavitation appearing ahead of the delamination front.

We have seen that the adhesion energy in a cleavage opening can be lower than 0.2kJ/m². This was found for all interlayers in a range of low temperatures or high loading speeds relative to their glass transition. Importantly, in the application we do not apply a constant displacement rate so that there is no risk of catastrophic failure in the field. However, for building applications this low adhesion could result in inaesthetic delamination.

The comparison between the rheology and the DBC experiments allowed us to link qualitatively the variation of the loss factor $\tan(\delta) = E''/E'$ and the variations of the adhesion energy with time and temperature. We can now provide the following explanations for our observations:

1. At low temperature or high-speed relative to the glass transition, the rigid interlayer elastically transmits the energy provided to the system towards the interface leading to a low adhesion energy (<0.2kj/m²) and abrupt delamination when a critical energy is reached. This corresponds to the abrupt delamination regime.
2. As the temperature increases or the speed is reduced, the interlayer enters its glass transition, becomes softer and more viscous, dissipation increases. The onset of this large deformation regime is found for a modulus between 100 and 10MPa for all 3 interlayers. The energy provided to the system is no longer efficiently transferred to the interface but lost in the viscous stretching of the interlayer. This leads to a higher adhesion energy being recorded.
3. As the temperature further increases or the speed is even further reduced, the interlayer is beyond its glass transition. The interlayer is still soft, and we still are in the large deformation delamination regime, but viscous dissipation has also decreased. During the DCB, the interlayer is submitted to large deformations, but the lower viscous dissipation leads to lower recorded adhesion energy as visible for the standard PVB above temperatures of 20°C and characteristic times longer than 1s. Further experiments are required to confirm the same phenomenon on the structural PVB.

For the ionomer, the crystallites present in the interlayer are melting at 80°C leading to higher mobility of the polymer chains that could affect the adhesion of the ionomer to glass. Combined with the plastic behavior of the ionomer interlayer this could explain the adhesion energy that remains higher than 1kJ/m² even for temperature above the glass transition temperature. We would need to conduct additional experiments to check these possible explanations.

Finally, this analysis based on small strain rheology only describes qualitatively the temperature/speed dependence of the adhesion energy. Large strain mechanical properties should obviously be considered in modelling the adhesion of the interlayers in the DCB experiment. The link between the size of the cavitation zone and the rheological properties of the interlayer has not been investigated here and could be linked to the high adhesion energy measured at the glass transition.

Acknowledgements

We would like to thank Vincent Leboeuf, Aurélien Gouy and Christophe Swiderski for the sample preparations and for the DCB experiments. We would also like to thank Elodie Couttenier for the sample preparation with the ionomer interlayer and the technical discussions.

References

Biolzi, L. et al., 2014. Long term response of glass-PVB double lap joints. *Composites: Part B,* Volume 63, pp. 41-49.

Biolzi, L. et al., 2020. Constitutive relationships of different interlayer materials for laminated glass. *Composite Structures,* Volume 224, p. 112221.

Blackman, B. & Kinloch, A., 2001. Fracture Tests for Structural Adhesive Joints. In: P. A., D. Moore & J. Williams, eds. *Fracture Mechanics Testing Methods for Polymers, Adhesives and Composites.* s.l.:Elsevier.

Blackman, B., Kinloch, A., Taylor, A. & Wang, Y., 2000. The impact wedge-peel performance of structural adhesives. *Journal of Material Science,* Volume 35, pp. 1867-1884.

Briccoli Bati, B., Rannocchiai, G., Reale, C. & Rovero, L., 2009. Time-Dependent Behavior of Laminated Glass. *Journal of Materials in Civil Engineering,* 22(4).

Butchart, C. & Overend, M., 2012. Delamination in fractured laminated glass. *International Conference Glasstec.*

Centelles, X., Castro, J. & Cabeza, L., 2020. Double lap shear test on laminated glass specimens under diverse ageing conditions. *Construction and Building Materials,* 249(1981), p. 118784.

Centelles, X. et al., 2021. Viscoelastic characterization of seven laminated glass interlayer materials from static tests. *Construction and Building Materials,* Volume 279.

Chung, J. & Chaudury, M., 2005. Soft and Hard Adhesion. *The Journal of Adhesion,* Volume 81, pp. 1119-1145.

Corroyer, E., Brochier-Salon, M. C., Chaussy, D. & Wery, S., 2013. Characteriszation of commercial polyvinylbutyrals. *International journal of polymer analysis and characterization,* 18(5), pp. 345-357.

Decourcelle, R., 2011. Comportement mécanique des vitrages feuilletés sous chargements statiques et dynamiques. s.l.:PhD - Université de Rennes 1.

Decourcelle, R., Nugue, J. & Levasseur, F., 2009. Mechanical participation of interlayer on laminated glass for building applications. *Glass Performance Days.*

Delince, D. et al., 2008. Experimental investigation of the local bridging behaviour of the interlayer in broken laminated glass. *International Symposium on the Application of Architectural Glass Munich,* pp. 41-49.

Elziere, P., 2016. Laminated glass: dynamic rupture of adhesion. *PhD.*

Elziere, P. et al., 2017. Large strain viscoelastic dissipation during interfacial rupture in laminated glass. *Soft Matter,* Volume 13, pp. 1624-1633.

Elziere, P. et al., 2019. Supramolecular Structure for Large Strain Dissipation and Outstanding Impact Resistance in Polyvinylbutyral. *Macromolecules,* 52(20), pp. 7821-7830.

Ferretti, D., Rossi, M. & Carfagni, G., 2012. Through-Cracked Tensile Delamination Tests with Photoelastic Measurements. *Challenging Glass Conference 3.*

Fourton, P., Piroird, K., Ciccotti, M. & Barthel, E., 2020. Adhesion rupture in laminated glass: influence of adhesion on the energy dissipation mechanisms. *Glass Structures & Engineering,* Volume 5, pp. 397-410.

Hooper, P. & Blackman, B., 2012. The mechanical behavior of poly(vynil butyral) at different strain magnitudes and strain rates. *Journal of Material Science,* Volume 47, pp. 3564-3576.

Huntsberger, J., 1981. Adhesion of plasticized Poly(Vinyl Butyral) to Glass. *Journal of Adhesion,* Volume 13, pp. 107-129.

Jagota, A., Bennison, J. & Smith, C., 2000. Analysis of a compressive shear test for adhesion between elastomeric polymers and rigid substrate. *International Journal of Fracture,* Volume 104, pp. 105-130.

Juang, Y., Lee, L. & Koelling, K., 2001. Rheological Analysis of Polyvinyl Butyral Near the Glass Transition Temperature. *Polymer Engineering and Science,* 41(2), pp. 275-292.

Moreno, C., Piroir, K. & Lorenceau, E., 2022. Extended time–temperature rheology of polyvinylbutyral (PVB). *Rheologica Acta,* Volume 61, pp. 539--547.

Mostovoy, S. R. E., 1966. Fracture Toughness of an Epoxy System. *Journal of Applied Polymer Science,* Volume 10, pp. 1351-1371.

P., H. & Oechsner, M., 2017. Testing of Adhesion on Laminated Glass Using Photometric Measurements. *Glass performance days .*

Pelfrene, J., Van Dam, S. & Van Paepegem, W., 2015. Numerical analysis of the peel test for characterisation of interfacial. *International Journal of Adhesion & Adhesives,* Volume 62, pp. 146-153.

Poblete, F. et al., 2022. Direct measurement of rate-dependent mode I and mode II traction-separation laws for cohesive zone modeling of laminated glass. *Composite Structure,* Volume 279, p. 114759.

Rahul-Kumar, P., Jagota, A., Bennison, S. & Saigal, S., 2000. Interfacial failures in a compressive shear strength test of glass/polymer laminates. *International Journal of Solids and Structures,* 37(48).

Samieian, M. et al., 2019. On the bonding between glass and PVB in laminated glass. *Engineering Fracture Mechanics,* Volume 214, pp. 504-519.

Santarsiero, M., Louter, C. & Nussbaumer, A., 2016. The mechanical behaviour of SentryGlas® ionomer and TSSA silicon bulk materials at different temperatures and strain rates under uniaxial tensile stress. *Glass Structures and Engineering,* Volume 1, pp. 395--415.

Santarsiero, M., Louter, C. & Nussbaumer, A., 2017. Laminated connections under tensile load at different temperatures and strain rates. *International Journal of Adhesion and Adhesives,* Volume 79, pp. 23-49.

Schuster, M., 2022. Determination of the linear viscoelastic material behaviour of interlayers with semi-crystalline structures shown by the example of a semi-crystalline ionomer. *Glass Structures & Engineering,* Volume 7, pp. 157-171.

Schuster, M., Schneider, J. & Nguyen, T., 2020. Investigations on the execution and evaluation of the Pummel test for polyvinyl butyral based interlayers. *Challenging Glass,* Volume 5, pp. 371-396.

Seshadri, M., Bennison, S., Jagota, A. & Saigal, S., 2002. Mechanical response of cracked laminated glass. *Acta Materialia,* Volume 50, pp. 4477-4490.

Sha, Y. et al., 1997. Analysis of adhesion and interface debonding in laminated safety glass. *Journal of Adhesion Science and Technology,* 11(1), pp. 49-63.

Stevels, W., D'Haene, P. & Haldeman, S., 2016. A Comparison of Different Methodologies for PVB Interlayer Modulus Characterization. *Challenging Glass 5 – Conference on Architectural and Structural Applications of Glass.*

Su, Y. et al., 2022. Surlyn resin ionic interlayer-based laminated glass: preparation and property. *Advanced Composites and Hybrid Materials,* Volume 5, pp. 229-237.

Wiechter., E., 1893. Gesetze der elastischen nachwirkung für constante temperatur.. *Annalen der Physik,* 286(10), p. 335–348.

Williams, M., Landel, R. & Ferry, J., 1955. The temperature dependence of relaxation mechanisms in amorphous polymers and other glass forming liquids.. *Journal of the American Chemical Society,* 77(14), p. 3701–3707.

Xie, D. et al., 2022. Thermal Rheological Behavior of Composite Interlayer in Laminated Glass. *Challenging Glass Conference Proceedings - Volume 8.*

Xie, D., Yang, J., Zhao, C. & Wang, X., 2024. Comprehensive investigation into the thermal rheological behavior and relaxation characteristic of single/composite polymers in laminated glass. *Thin-Walled Structures,* Volume 195, p. 111369.

Yang, J. et al., 2023. Constitutive models for temperature-, strain rate and time-dependent behaviors of ionomers in laminated glass. *Journal of Materials Science,* Volume 58, pp. 3608-3624.

Challenging Glass Conference Proceedings – Volume 9 – June 2024 – Louter, Bos & Belis (Eds.)
International Conference on the Architectural and Structural Application of Glass
Challenging Glass Conference 9 – 19 & 20 June 2024 – TU Delft – The Netherlands

Platinum Sponsor

SAINT-GOBAIN

Gold Sponsors

EASTMAN kuraray sedak

Silver Sponsors

DOW® octatube PERMASTEELISA GROUP

Organising Partners

TU Delft Delft University of Technology

Technical University of Munich

GHENT UNIVERSITY